POLYOXOMETALATES

Open Access
RESEARCH ARTICLE

Composite membranes of quaternary ammonium cationic grafting poly(benzimidazole) modified by molybdenum clusters with enhanced proton conductivity

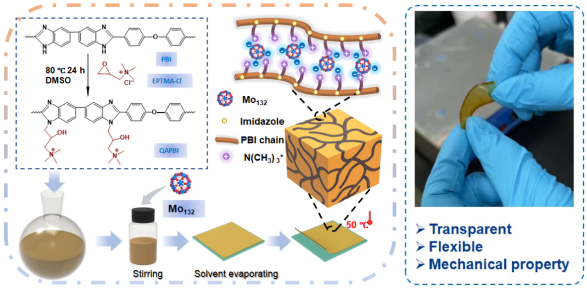
Wen-Hang Guo[1,2], Feng-Zhi Wang[1], Chen Wang[3], Zhen-Ning Liu[1], Yun-Zuo Cui[2], Wen Tang[3], Song Liang[1] ✉, and Hong-Ying Zang[2] ✉

[1] *Key Laboratory of Bionic Engineering (Ministry of Education), College of Biological and Agricultural Engineering, Jilin University, Changchun 130022, China*
[2] *Key Laboratory of Polyoxometalate and Reticular Material Chemistry of Ministry of Education at Universities of Jilin Province, Faculty of Chemistry, Northeast Normal University, Changchun 130024, China*
[3] *College of Chemistry and Chemical Engineering, Huangshan University, Huangshan 245042, China*

Cite This: *Polyoxometalates*, **2026**, *5*, 9140136

Read Online

ABSTRACT: Developing novel, low-cost, and high-performance proton exchange membranes (PEMs) to replace commercial Nafion is of great significance. By grafting quaternary ammonium cations onto the side chains of polybenzimidazole, abundant charge carriers and proton hopping sites are provided for proton transport, accelerating proton migration and thereby enhancing the proton conductivity of composite membranes made from this material. Furthermore, polyoxometalates (POMs) are introduced through electrostatic interactions, and their exceptional proton-conducting properties further improve the proton conductivity of the composite membranes, with the maximum proton conductivity reaching 0.123 S·cm^{-1}. This work demonstrates that POM-based materials can serve as excellent proton carriers, expanding the selection of active materials for composite membranes and providing new references for the fabrication of novel proton exchange membranes.



KEYWORDS: polyoxometalates, proton exchange membranes, quaternary ammonium cationic, proton conduction

1 Introduction

Proton exchange membranes (PEMs) are crucial leading materials driving energy transformation and green development in the fields of energy conversion and storage [1–3]. PEM fuel cells are promising devices for replacing traditional fossil energy sources as they are highly efficient and clean. As the core component of these fuel cells, the PEM, much like the membrane of a biological cell, undertakes the critical roles of proton conduction and electron isolation. In recent years, researchers have steadily overcome technical bottlenecks to enhance the performance of PEMs [4–7]. The application of novel materials has led to significant progress in durability, high-temperature resistance, and corrosion resistance. In 2024, a polyoxometalate (POM)-based material, 2MeIm-Mo_{132}, was introduced into a SPAEKS substrate to prepare high-performance PEMs, which exhibited a high proton conductivity of 75 mS·cm^{-1} and were applied to PEM fuel cells [8]. The results demonstrated that POM-based materials can act as effective proton conduction sites, providing new insights into the application of POM-based materials in the PEM field.

POMs are compounds with unique structures formed through coordination bonds between metal and oxygen atoms [9–11]. Their diverse architectures and high stability are of significant interest in areas such as catalysis and energy storage [12–15]. Within the scope of PEM applications, POM-based materials exhibit distinct advantages [16–18]. First, POM-based materials exhibit excellent proton conductivity, and the oxygen atoms and metal ions within their structure form abundant proton-transport pathways, effectively enhancing membrane conductivity and thereby boosting the fuel-cell power output. Second, POM-based materials exhibit notable thermal and chemical stability, enabling them to maintain consistent proton conductivity even under harsh conditions like elevated temperatures and humidity. This stability extends the operational lifespan of POM-based PEMs. Furthermore, incorporating POM-based materials can also enhance the mechanical robustness of the membrane, improving its durability. Consequently, integrating POM-based materials into PEMs is a promising strategy for developing advanced membranes with

Received: March 16, 2026; **Revised:** April 14, 2026
Accepted: May 7, 2026

✉Address correspondence to Song Liang, songliang@jlu.edu.cn; Hong-Ying Zang, zanghy100@nenu.edu.cn

https://doi.org/10.26599/POM.2026.9140136

superior performance, which will help further advance fuel-cell technology.

In this work, molybdenum clusters {Mo_{132}} were introduced into QAPBI (quaternary ammonium (QA) cation-grafted polybenzimidazole (PBI)) chains to prepare composite membranes. The optimal QAPBI formulation shows excellent proton conductivity (0.123 S·cm^{-1} at 353 K). The electrostatic interactions provided by {Mo_{132}} and QA cations provide additional proton-transport channels that increase the proton-transfer rate. This work elucidates and validates a universal design strategy of using covalently grafted cationic side chains as electrostatic anchors for POMs. This synergistic strategy effectively achieves high loading, superior retention, and enhanced proton conduction, providing a new avenue for developing high-performance composite PEMs.

2 Results and discussion

The polyhedral structure of the {Mo_{132}} POM is shown in Fig. S1 in the Electronic Supplementary Material (ESM). The basic structure is composed of twelve pentagonal {Mo_6} and 30 edge-sharing {Mo_2} basic building units. Molybdenum atoms exist in both +5 and +6 oxidation states in {Mo_{132}}, including 60 Mo^{V} and 72 Mo^{VI} atoms, respectively, among which, 30 Mo^{VI} atoms are from 10 {Mo_3} structural units, and 10 Mo^{V} atoms are from the {Mo_{90}} ring [19]. In this work, 2,3-epoxypropyltrimethyl ammonium chloride (EPTMA-Cl) was used as a quaternization reagent and grafted onto the side chains of PBI through a ring-opening reaction to synthesize QAPBI with QA side chains that bear terminal hydroxyl groups to increase the number of active sites in the polymer matrix. Then, a series of QAPBI-based composite PEMs were prepared by adding different mass fractions of the {Mo_{132}} POM into QAPBI (Figs. 1 and 2). The corresponding preparation schemes of PBI-*x* and ionic liquid (IL)/PBI-*x* composite membranes are shown in Figs. S2 and S3 in the ESM.

The side-chain functionalization of PBI polymers using QA cations offers the following significant advantages [20, 21]: (i) QA groups exhibit superior proton conductivity compared to other cationic groups; (ii) the N–H groups on the PBI backbone serve as excellent active sites for grafting QA cation side chains; (iii) the $N(CH_3)_3^+$ groups on the QA side chains readily interact with the negatively charged {Mo_{132}} through electrostatic interactions; (iv) by introducing QA side chains into the PBI polymer backbone, the hydrophilicity and proton conductivity of the composite membrane can be increased while simultaneously enhancing its mechanical strength and durability.

The chemical structure of the prepared QAPBI polymer was characterized using proton nuclear magnetic resonance (^{1}H NMR) spectroscopy. The signals in the range of 7.0–8.5 ppm in the ^{1}H NMR spectrum (Fig. 3(a)) correspond to the characteristic peaks of the hydrogen atoms in the aromatic rings of the PBI backbone. The singlet at 1.3 ppm and the doublet at 3.3 ppm correspond to the characteristic peaks of the hydrogen atoms on the methyl and methylene groups, respectively, in the QA side chain. Additionally, the characteristic peak at 4.6 ppm is attributed to the hydrogen atoms on the tertiary carbon of the side chain, whereas the signal at 6.1 ppm originates from the hydroxyl group at the end of the QA side chain. The observation of the characteristic peak related to the hydroxyl in the QA side chain confirms that EPTMA-Cl was successfully grafted onto the PBI backbone structure through a ring-opening reaction. These results demonstrated that QAPBI polymers were successfully synthesized using PBI and EPTMA-Cl as precursors.

Figure 3(b) shows the FT-IR spectra for {Mo_{132}}, PBI, QAPBI, and QAPBI-10, in which the characteristic absorption peak at 1319 cm^{-1} corresponds to the stretching vibration of the C–H bonds in the methyl and methylene groups of the QA side chains. A

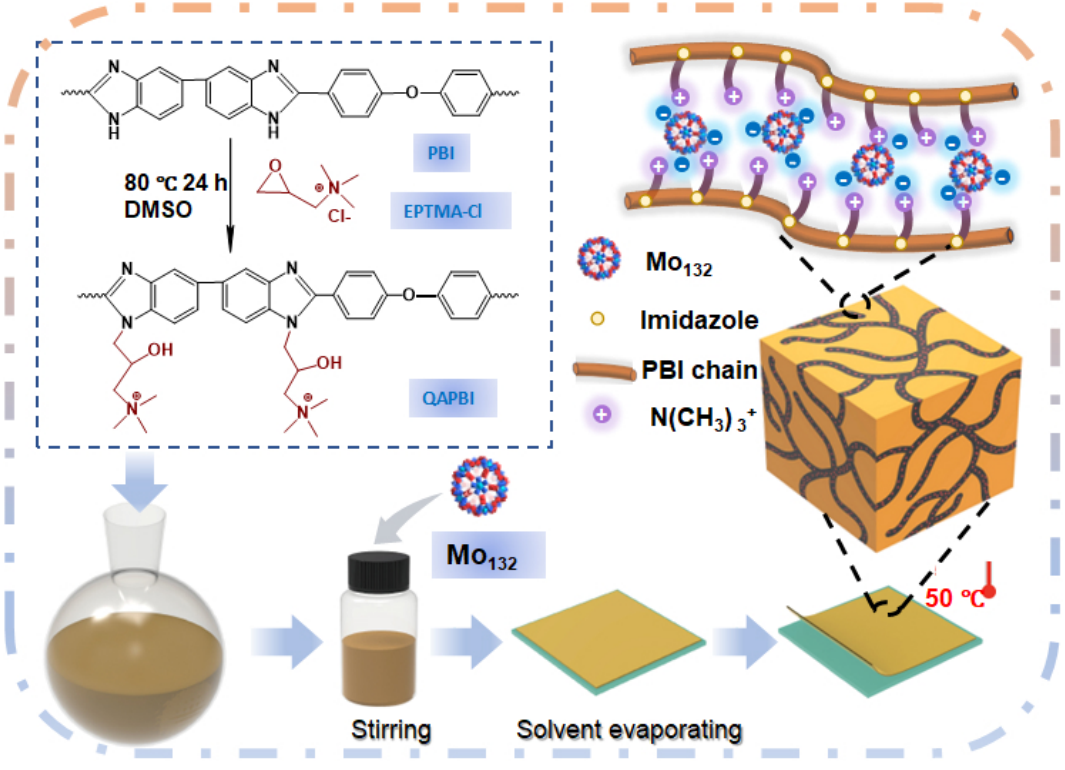


Figure 1 Preparation scheme of quaternary ammonium side chain branch PBI and QAPBI-*x* composite membranes.

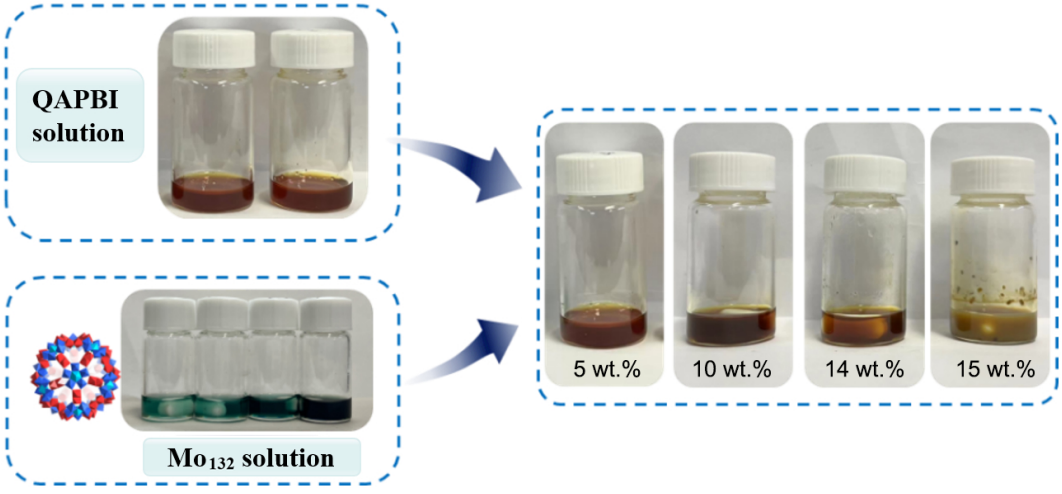


Figure 2 The photograph of QAPBI solutions, {Mo_{132}} solutions and QAPBI-*x* solutions.

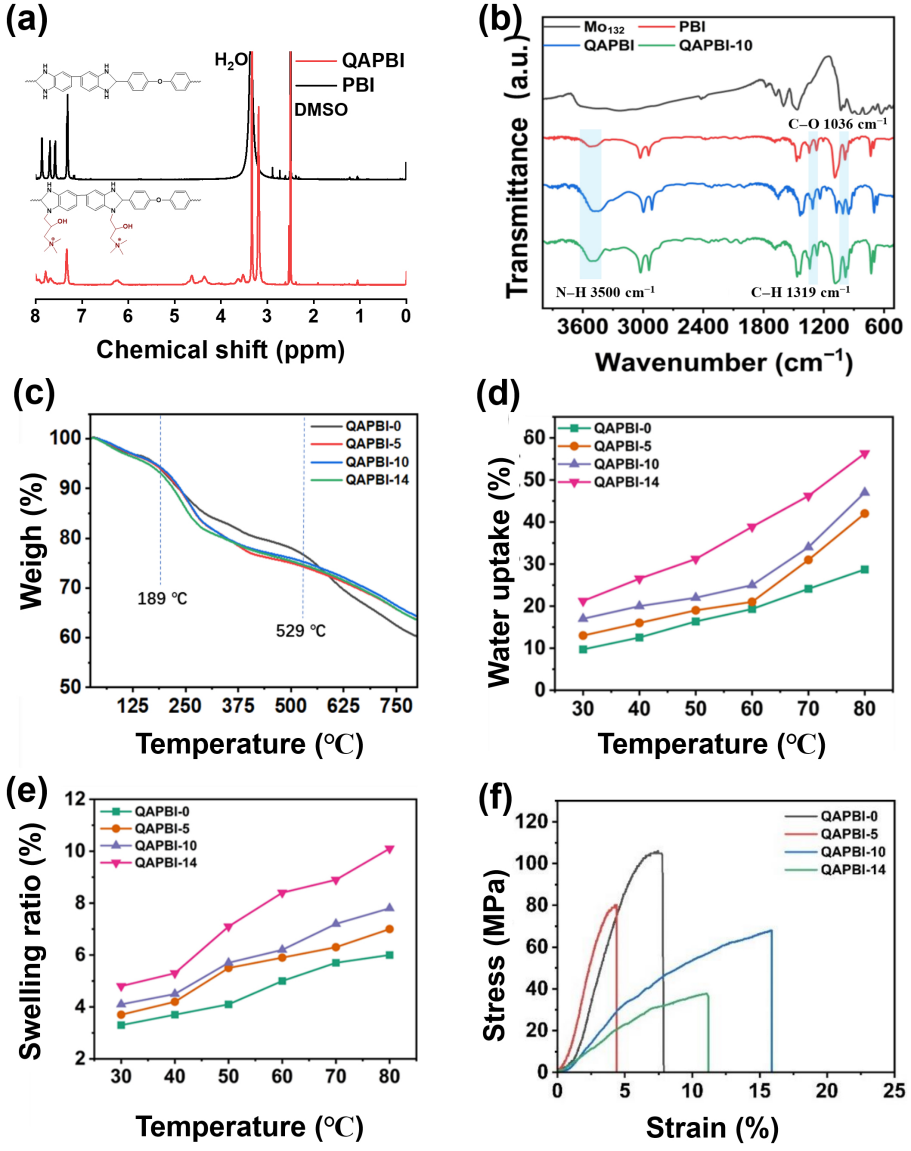


Figure 3 (a) ^{1}H NMR spectra of QAPBI and PBI. (b) FT-IR spectra of {Mo_{132}}, PBI, QAPBI, and QAPBI-10. (c) TGA curves of QAPBI-*x* composite membranes. (d) The water sorption of QAPBI-*x* composite membranes as a function of temperature. (e) The swelling rate of QAPBI-*x* composite membranes as a function of temperature. (f) Stress–strain curves of QAPBI-*x* composite membranes.

characteristic peak for the stretching vibration of the secondary alcohol C–O bond in the QA side chain is observed at 1036 cm^{-1}, whereas this peak is not observed in the PBI spectrum. The FT-IR spectral analysis confirms that EPTMA-Cl was successfully grafted onto the imidazole ring of the PBI polymer. The characteristic bands in the $\{Mo_{132}\}$ spectrum, arising from the symmetric and asymmetric vibrations of Mo=O and the stretching vibration of Mo–O–Mo, represent the typical metal-oxide framework of $\{Mo_{132}\}$. These characteristics peaks are observed in the QAPBI-10 spectrum, confirming that $\{Mo_{132}\}$ clusters maintain their structural integrity in the composite membranes. Additionally, compared to the spectrum for pure $\{Mo_{132}\}$, a shift in the N–H peaks between 3300–3500 cm^{-1} is observed in the spectra for all QAPBI-*x* composite membranes, indicating a change in the chemical environment around $\{Mo_{132}\}$. This is attributed to the electrostatic interactions between the negative charge of $\{Mo_{132}\}$ and the positive charge of the imidazole and QA groups in QAPBI. The above analysis further supports the successful incorporation of $\{Mo_{132}\}$ into the QAPBI backbone. The corresponding FT-IR spectra for the PBI-*x* and ILs/PBI-*x* samples are shown in Fig. S4 and S5 in the ESM, respectively.

The thermal stability of QAPBI-*x* composite membranes during long-term operation was investigated using thermogravimetric analysis (TGA). As shown in Fig. 3(c), the weight loss process of QAPBI-*x* occurs in three stages. The first stage at 50–189 °C is attributed to the loss of residual water and solvents within the QAPBI-*x* composite membranes. The second weight loss stage occurs at 189–529 °C, where the thermal decomposition of QAPBI primarily begins above 200 °C. All QAPBI-*x* membranes containing $\{Mo_{132}\}$ exhibit a higher rate and a greater percentage of weight loss than pure PBI composite membranes. Above 200 °C, the grafted QA side chains on the QAPBI start to break, and the end groups of PBI and $\{Mo_{132}\}$ begin to decompose. The third weight loss stage occurs above 529 °C, corresponding to the further decomposition of the PBI backbone. Ultimately, all QAPBI-*x* composite membranes retain more than 55% of their initial weight at *X* °C, and the composite membranes with added $\{Mo_{132}\}$ retain a greater proportion of their initial mass. The higher mass retention of the $\{Mo_{132}\}$-containing membranes at high temperatures (> 529 °C) suggests that the molybdenum-oxo clusters enhance the thermal stability of the composite. This is attributed to several potential mechanisms: (i) The inorganic $\{Mo_{132}\}$ clusters may act as physical cross-linking points within the polymer matrix, restricting chain mobility and thereby retarding the thermal degradation of the PBI backbone; (ii) $\{Mo_{132}\}$ could serve as a thermal stabilizer during pyrolysis, promoting the formation of a more stable carbonaceous residue that protects the underlying material; and (iii) the intrinsic high thermal stability of the polyoxometalate clusters contributes to the overall stability of the composite. This enhanced thermal stability is beneficial for the potential high-temperature operation of PEMs. The corresponding TGA curves of the PBI-*x* and ILs/PBI-*x* composite membranes are shown in Figs. S6 and S7 in the ESM, respectively.

Water is the primary carrier for proton transport, and hydrophilic composite membranes exhibit better proton conductivity. Therefore, the water uptake and swelling ratio of the QAPBI-*x* membranes as a function of temperature are shown in Fig. 3(d) and 3(e), respectively. The water uptake and swelling ratio increase with increasing temperature, and the composite membranes with added $\{Mo_{132}\}$ exhibit higher values than the pure QAPBI membranes at the same temperature. This is attributed to the abundant oxygen atoms on the surface of $\{Mo_{132}\}$, which can form hydrogen bonds with water molecules, thereby enhancing the water retention capability of the QAPBI membranes. Table S1 shows that the water uptake of QAPBI-*x* membranes increases faster than that of PBI-*x* membranes upon heating, which is attributed to the QA groups in the side chains of QAPBI that can interact electrostatically with $\{Mo_{132}\}$ and retain more $\{Mo_{132}\}$ molecules, leading to improved water retention in the composite membranes. The QAPBI-*x* composite membranes maintain a low swelling ratio despite their high water uptake. This good dimensional stability is attributed to the electrostatic interactions formed by acid–base pairs inhibiting polymer-chain movement. The corresponding water uptake and swelling ratio data for the PBI-*x* and ILs/PBI-*x* membranes are shown in Fig. S8 and S9 in the ESM, respectively.

The stress–strain curves in Fig. 3(f) show that the QAPBI-*x* composite membranes exhibit lower tensile strength and elongation compared to the pure PBI membrane. This is attributed to the introduction of QA side chains into the PBI backbone, which disrupts hydrogen bonding interactions between the imidazole groups. Compared to the pure QAPBI membranes, the QAPBI membranes with added $\{Mo_{132}\}$ exhibit lower tensile strength and elongation at break. This is attributed to the composite membranes being rich in hydrophilic QA side chains and $\{Mo_{132}\}$, which absorb water molecules from the air, reducing the mechanical strength of the composite membranes. Among them, QAPBI-10 exhibits the best overall mechanical properties, maintaining a tensile strength of 67.6 MPa, which is an improvement over the tensile strength of 65.4 MPa measured for the PBI-10 composite membrane (Fig. S10 in the ESM). The comprehensive mechanical properties and tensile strength of QAPBI-10 are not inferior to those of previously reported PEM materials [22–24]. The stress–strain curves for PBI-*x* and ILs/PBI-*x* membranes are shown in Figs. S10 and S11 in the ESM, respectively.

Scanning electron microscopy (SEM) images were obtained to investigate the microstructure of the PBI-*x*, QAPBI-*x*, and ILs/PBI-*x* composite membranes. The SEM images of the QAPBI-0 and QAPBI-10 composite membranes are shown in Fig. S12 in the ESM. The surface morphologies of both PEMs obtained under various magnifications suggest uniform and dense membranes. The cross-section of the QAPBI-10 film is more compact and dense and exhibits a layered texture (Fig. S12(f) in the ESM), which may be attributed to the grafting of QA side chains on PBI, which can enhance the electrostatic interactions between QAPBI and $\{Mo_{132}\}$, leading to the formation of an ordered molecular structure in the composite membrane. The SEM images of PBI-*x* and ILs/PBI-*x* are shown in Figs. S13 and S14 in the ESM, respectively. Figure 4(a) shows energy dispersive spectroscopy (EDS) maps of elements C, N, O, Cl, and Mo measured at the surfaces of the QAPBI-*x* composite membranes, whereas Fig. 4(b) shows the same results for a cross-section of the QAPBI-10 composite membrane. The EDS distribution maps show that Cl is relatively uniformly distributed on both the surface and cross-section of the QAPBI-10 composite membrane, indicating that the flexible QA side chains were successfully grafted onto the PBI main chains and provide uniformly abundant active sites for binding with $\{Mo_{132}\}$ molecules. As shown in Fig. 4(a), Mo is relatively uniformly distributed through the composite membranes, and no obvious aggregation is detected. More importantly, the uniform co-distribution of Cl (QA

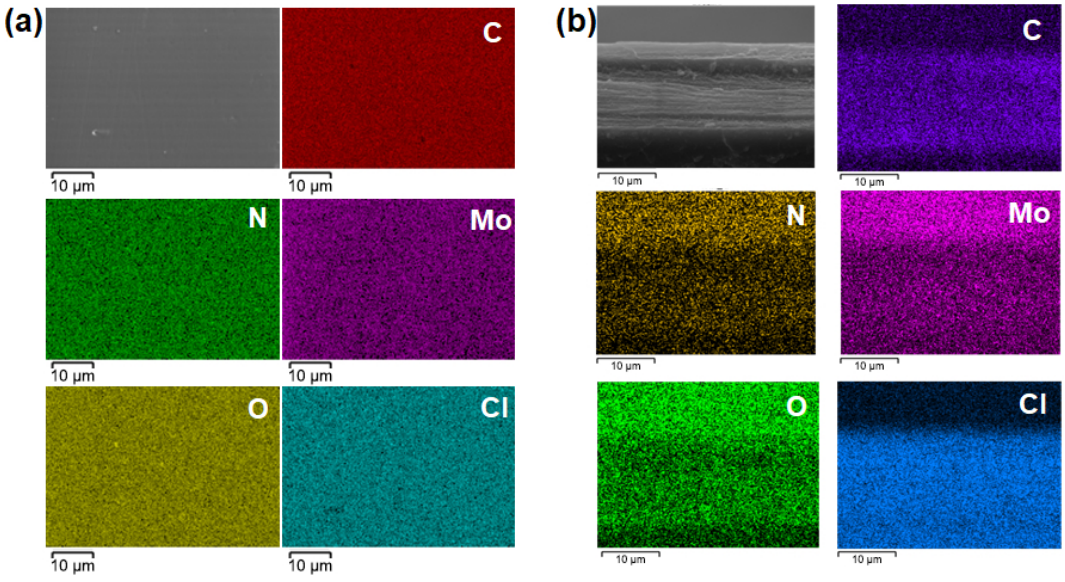


Figure 4 (a) SEM image and EDS mapping on the surface of QAPBI-10 composite membranes. (b) SEM image and EDS mapping of the cross-section on QAPBI-10 composite membranes.

sites) and Mo ($\{Mo_{132}\}$) from the microscale to the nanoscale is crucial for constructing a continuous, interpenetrating proton-transport network throughout the entire membrane. This structure ensures a uniform and high-density distribution of proton-hopping sites (QA groups) and rapid proton relays $\{Mo_{132}\}$ in three-dimensional space, thereby minimizing the tortuosity of the proton-transport path and associated energy barriers. This is a key structural foundation for the high proton conductivity (0.123 S·cm^{-1}) achieved by the QAPBI-10 membrane. The EDS maps of the PBI-*x* and ILs/PBI-*x* composite membranes are shown in Figs. S15 and S16 in the ESM, respectively. Furthermore, an element analyzer was used to investigate the content and stability of $\{Mo_{132}\}$ molecules within the composite membranes to evaluate their retention performance. As shown in Fig. S17 in the ESM, the contents of $\{Mo_{132}\}$ in the PBI-10, QAPBI-10, and ILs/PBI-15 composite membranes are 7.47%, 9.38%, and 13.06%, respectively. This demonstrates that the QAPBI-10 composite membrane can immobilize more $\{Mo_{132}\}$ molecules than the PBI-10 membrane, which is attributed to the electrostatic interactions between the QA side chains and $\{Mo_{132}\}$ molecules. After immersion treatment in water, the QAPBI-10 composite membrane retains more $\{Mo_{132}\}$ molecules, which supports our initial hypothesis during the experimental design.

The proton conductivity curves for QAPBI-*x*, PBI-*x*, and ILs/PBI-*x* composite membranes as a function of temperature (Figs. 5(a) and Figs. S18–S20 in the ESM) show that the proton conductivity is positively correlated with temperature. This is attributed to enhanced rates of proton transport at higher temperatures. The proton conductivity initially increases and then decreases with increasing $\{Mo_{132}\}$ content (Table S2 in the ESM). This trend is also clearly observed for the ILs/PBI series, where the conductivity reaches an optimum for ILs/PBI-15 (0.252 S·cm^{-1}) and then slightly declines for ILs/PBI-20 (0.238 S·cm^{-1}). This decrease is attributed to the aggregation of $\{Mo_{132}\}$ clusters at excessive loading (20 wt.%), which disrupts the continuity and uniformity of proton-transport pathways. The corresponding decrease in ion exchange capacity (IEC) and increase in activation energy for ILs/PBI-20 (Table S2 in the ESM) support this explanation, indicating a reduction in effective proton sites and a higher energy barrier for proton transport. The QAPBI-10 composite membrane exhibits the best proton conduction performance, achieving a proton conductivity of 0.123 S·cm^{-1} at 353 K, compared to 0.014 S·cm^{-1} for the PBI-10 membrane. The enhanced proton conductivity of QAPBI-10 is attributed to the introduction of QA groups into the PBI backbone, which improves the anti-swelling and mechanical properties and provides abundant ion-exchange groups. Additionally, the proton conductivity of the QAPBI-*x* membranes is enhanced by the electrostatic interactions between the $N(CH_3)_3^+$ groups and the negative charge of $\{Mo_{132}\}$, resulting in a stronger binding affinity and higher retention capacity for $\{Mo_{132}\}$.

However, when the $\{Mo_{132}\}$ content increases to 14 wt.%, the proton conductivity begins to decrease, because the excessive addition of $\{Mo_{132}\}$ leads to uneven dispersion and aggregation. In addition to aggregation, the notably high water uptake of 56.31% for QAPBI-14 at 80 °C (Table S1 in the ESM) suggests excessive membrane swelling at elevated $\{Mo_{132}\}$ loading, which can disrupt the continuity and compactness of the proton-conducting pathways, as inferred from the comparative cross-sectional morphology of QAPBI-10 (Fig. S12 in the ESM). The comprehensive results—including evidence of filler aggregation, excessive hydration, and potential morphological limitations—provide a detailed explanation for the observed trend in proton conductivity versus $\{Mo_{132}\}$ content. Comparatively, the ILs/PBI-*x* series exhibits higher overall proton conductivity, reaching 0.252 S·cm^{-1} for ILs/PBI-15 (Table S2 in the ESM). This superior conductivity is primarily attributed to the presence of the IL $[BMIM]BF_4$, which acts as an excellent proton solvent and provides highly continuous ionic channels, thereby facilitating Grotthuss and vehicle mechanism-based proton transport. However, the conductivity of ILs/PBI-20 is lower (0.238 S·cm^{-1}), with the conductivity versus $\{Mo_{132}\}$ content curve following a similar volcano-type trend to that observed for the QAPBI-*x* series, which is likely due to the aggregation of excess $\{Mo_{132}\}$. The key distinction between the two series lies in the long-term stability and retention of the active component. While the ILs/PBI-*x* membranes achieve higher initial conductivity through physical blending, the

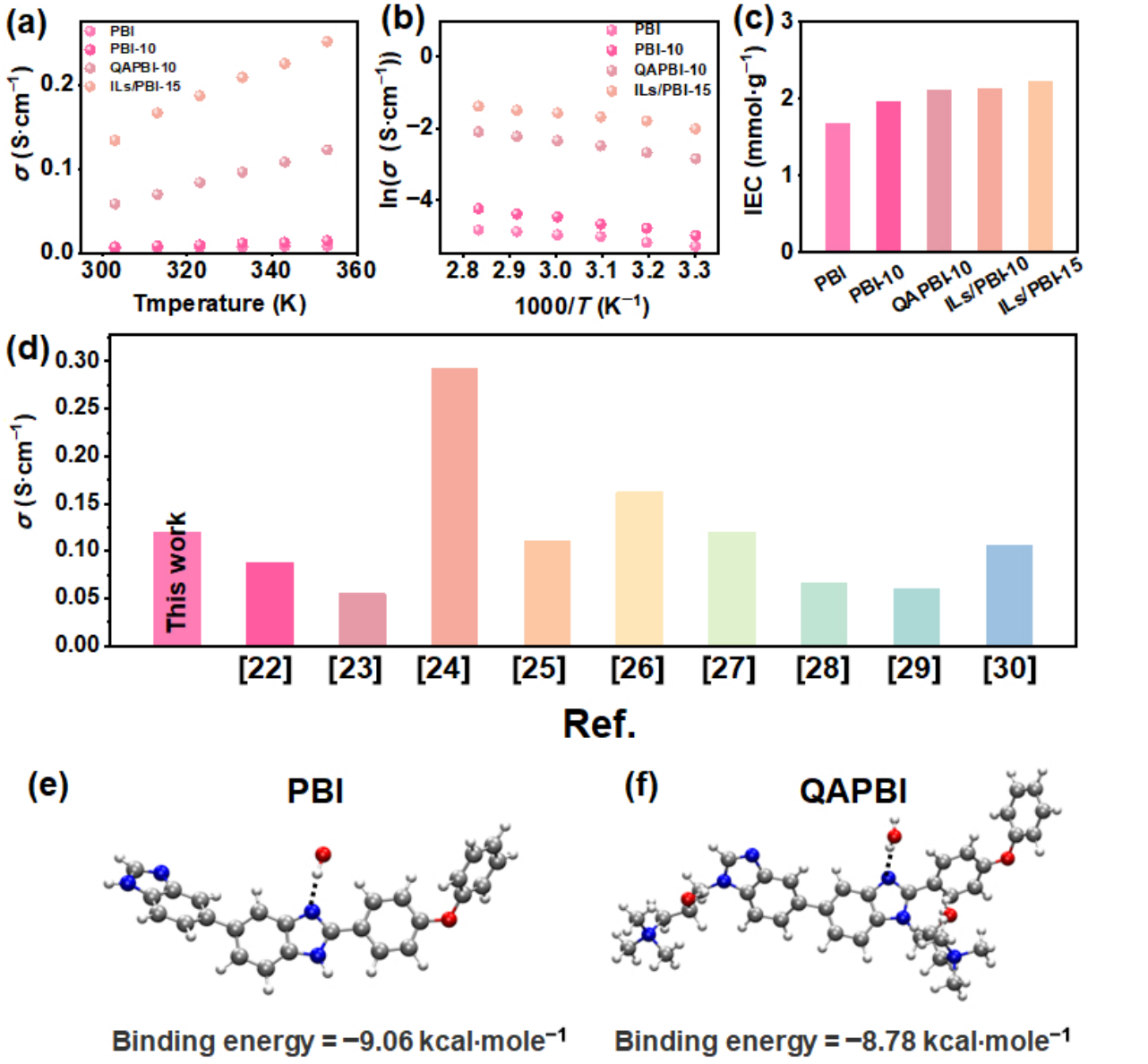


Figure 5 (a) The proton conductivity of PBI, PBI-10, QAPBI-10, and ILs/PBI-15 composite membranes as a function of temperature. (b) Arrhenius plots of PBI, PBI-10, QAPBI-10, and ILs/PBI-15 composite membranes. (c) The IEC values of PBI, PBI-10, QAPBI-10, and ILs/PBI-15 composite membranes. (d) Comparison with others reported proton exchange membranes in proton conductivity. (e) The binding energy of PBI monomer with water molecule. (f) The binding energy of QAPBI monomer with water molecule.

QAPBI-*x* membranes leverage the covalent grafting of QA side chains to electrostatically anchor {Mo_{132}}, as evidenced by the higher {Mo_{132}} retention rate for QAPBI-10 (9.38%) than PBI-10 (7.47%) after water immersion (Fig. S17 in the ESM). This characteristic may endow the QAPBI-*x* membranes with better durability against component leaching during prolonged operation, addressing a common drawback of physically blended composite membranes.

The activation energies for PBI-*x*, QAPBI-*x*, and ILs/PBI-*x* with various {Mo_{132}} contents were calculated using the Arrhenius equation (Fig. 5(b) and Figs. S18–S20 in the ESM), giving activation energies of 21.57 and 12.31 kJ·mol^{-1} for the QAPBI-0 and QAPBI-10 membranes, respectively. The lower activation energy for QAPBI-10 indicates that the addition of an appropriate amount of {Mo_{132}} effectively reduces the energy barrier for proton transport, thereby enhancing the proton conductivity of the membrane. The IEC refers to the amount of exchangeable H^+ ions per unit mass of the composite membranes, which directly reflects the proton conductivity of the composite membranes. As shown in Fig. 5(c) and Figs. S21–S23 in the ESM, the IEC for the QAPBI-*x* composite membranes initially increases and then decreases with increasing {Mo_{132}} content, with a maximum IEC of 2.11 mmol·g^{-1} obtained for 10 wt.% {Mo_{132}}. This is attributed to the hydrophilicity of $N(CH_3)_3^+$ groups in the QA side chains, where the strong affinity between the $N(CH_3)_3^+$ groups and {Mo_{132}} enhances {Mo_{132}} absorption via electrostatic interactions, providing more protons in the aqueous solution and ultimately increasing the IEC of the QAPBI-*x* composite membranes. When the {Mo_{132}} content exceeds 10 wt.%, excess {Mo_{132}} molecules agglomerate within the composite membranes, hindering the dissociation of H^+ ions, resulting in a decrease in IEC. Furthermore, a comparison of proton conductivity performance with previously reported proton

exchange membranes (Fig. 5(d)) demonstrates that the prepared QAPBI-10 exhibits superior performance [25–33]. The results of theoretical calculations indicate that appending the QA cations onto the side chains of PBI polymers significantly reduces the binding energy with water molecules (PBI: −9.06 kcal/mole; QAPBI: −8.78 kcal·mol^{-1}). This modest reduction in binding energy indicates a slightly weaker, yet still favorable, interaction between the polymer and water molecules. This is beneficial for proton conduction because it implies a more dynamic and less tightly bound hydration shell. Such an environment facilitates both the reorganization of the hydrogen-bond network and the diffusion of water molecules, thereby lowering the overall energy barrier for proton transport (Figs. 5(e) and 5(f)). The modified QAPBI polymers maintain interactions with water molecules while preventing excessive adsorption, enabling the enhanced mobility of water molecules within the structure, thereby facilitating their rapid diffusion. In addition, the lower binding energy corresponds to weaker intermolecular forces, which reduce the energy barrier for water-molecule desorption, leading to enhanced water adsorption and desorption processes. Finally, the reduced binding energy suggests that the interaction between the QAPBI chains and water molecules is dynamic and reversible, enabling the efficient and rapid binding and release of water molecules. Collectively, these results demonstrate that branching the PBI side chains promotes the rapid transport of water molecules through QAPBI-*x* composite membranes, thereby enhancing proton conductivity.

3 Conclusion

QAPBI polymers were successfully prepared by adding QA side chains to PBI to overcome the excessive loss of active materials. QAPBI-*x* PEMs with various {Mo_{132}} contents were assembled for the first time using an electrostatic assembly strategy. This strategy is based on the synergistic effect between the grafted QA groups and {Mo_{132}} clusters; the dual-functional QA groups act as proton-hopping sites and electrostatic anchors that firmly immobilize the negatively charged {Mo_{132}}, while the {Mo_{132}} clusters provide additional proton-coupled electron-transfer characteristics and hydrophilic sites, collectively facilitating proton transport. Consequently, the assembled PEMs show improved {Mo_{132}} retention rate, proton conductivity, and mechanical strength, with the proton conductivity of QAPBI-10 reaching 0.123 S·cm^{-1} with a corresponding tensile strength of 67.6 MPa. The proposed strategy overcomes the typically low proton conductivity of quaternized PBI-based PEMs and provides a universal strategy for preparing such PEMs with high proton conductivity. To further assess the application potential of the proposed PEMs, subsequent studies should investigate their long-term durability and performance in practical fuel-cell devices.

Electronic Supplementary Material: Supplementary material (including experimental details, FT-IR, PXRD, and other characterization) is available in the online version of this article at https://doi.org/10.26599/POM.2026.9140136.

Data availability

All data needed to support the conclusions in the paper are presented in the manuscript and the Electronic Supplementary Material. Additional data related to this paper may be obtained from the corresponding author upon request.

Acknowledgements

This work was supported by the National Natural Science Foundation of China (No. 22322102), the National Key Research and Development Program of China (No. 2022YFE0138500), the Fundamental Research Funds for the Central Universities-Excellent Youth Team Program (No. 2412023YQ001), the Natural Science Foundation of Jilin Province (No. 20200201083JC), the Natural Science Foundation of the Department of Education of Jilin Province (No. JJKH20201169KJ), and the Scientific Research Foundation for Scholars of Huangshan University (No. 2025xkjq054).

Declaration of competing interest

The authors have no competing interests to declare that are relevant to the content of this article.

Author contribution statement

W.-H. G.: Data curation, writing manuscript. F.-Z. W. and C. W.: validation, experimental design. Z.-N. L., Y.-Z. C., and W. T.: writing manuscript. S. L. and H.-Y. Z.: Project administration, funding acquisition, writing manuscript. All authors contributed to the general discussion.

Use of AI statement

None.

References

[1] Feng, Y.; Wang, J. H.; Feng, K.; Xu, B.; Xu, J. B.; Li, S.; Lu, C.; Fan, X.; Lin, H. P.; Zhong, J. Breathing mode in Nd–CoO_x for active and stable proton exchange membrane water electrolysis. *Nat. Commun.* **2025**, *16*, 10998.

[2] Song, Z. X.; Zhang, Q. F.; Zhang, Y.; Wu, M. Y.; Liao, J. H.; Liu, X. Q.; Zhang, Z. Y.; Li, Y. L.; Ren, X. Z.; Zhang, L. et al. Regulating coordination environment of atomic dimer catalysts for high performance oxygen reduction reaction in fuel cells. *App. Catal. B: Environ.* **2025**, *365*, 124970.

[3] Liu, B. L.; Hu, B.; Du, J.; Cheng, D. M.; Zang, H. Y.; Ge, X.; Tan, H. Q.; Wang, Y. H.; Duan, X. Z.; Jin, Z. et al. Precise molecular-level modification of Nafion with bismuth oxide clusters for high-performance proton-exchange membranes. *Angew. Chem., Int. Ed.* **2021**, *60*, 6076–6085.

[4] Li, T. T.; Liu, B. H.; Chai, S. C.; Zuo, P.; Zhao, C. J.; Li, H. L. Highly conductive polymer electrolyte membranes with polyoxometalate hybrid nanodomains for high-temperature fuel cells. *Nano Lett.* **2025**, *25*, 11149–11155.

[5] He, H. B.; Song, S. H.; Zhai, L.; Li, Z. X.; Wang, S. H.; Zuo, P.; Zhu, Y. L.; Li, H. L. Supramolecular modifying Nafion with fluoroalkyl-functionalized polyoxometalate nanoclusters for high-selective proton conduction. *Angew. Chem., Int. Ed.* **2024**, *63*, e202409006.

[6] Zhai, L.; Chai, S. C.; Li, T. T.; Li, H. B.; He, S. Q.; He, H. B.; Li, X.; Wu, L. X.; Jiang, F. J.; Li, H. L. Self-assembled construction of ion-selective nanobarriers in electrolyte membranes for redox flow batteries. *Nano Lett.* **2023**, *23*, 10414–10422.

[7] Li, X.; Chai, S. C.; Zhai, L.; Guo, H. K.; He, H. B.; Li, H. B.; Wu, L. X.; Li, H. L. Semi-solid supramolecular ionic network electrolytes formed by zwitterionic liquids and polyoxometalate nanoclusters for high proton conduction. *Macromol. Rapid Commun.* **2023**, *44*, 2300223.

[8] Ji, F.; Jiang, F. Y.; Luo, H. W.; He, W. W.; Han, X.; Shen, W. W.; Liu, M. L.; Zhou, T.; Xu, J. M.; Wang, Z. et al. Hybrid membrane of sulfonated poly(aryl ether ketone sulfone) modified by molybdenum clusters with enhanced proton conductivity. *Small* **2024**, *20*, 2312209.

[9] Yang, Y. L.; Li, B. Q.; Wang, C.; Guo, K. K. Polyoxometalate-based MOF as a highly sensitive and stable X-ray detector for imaging. *Angew. Chem., Int. Ed.* **2025**, *64*, e202518832.

[10] Zhang, B. Y.; Wang, N. H.; Wu, X. S.; Tian, Y.; Wang, X. L.; Han, X. Q.; Su, Z. M. Building blocks selected via a rational design strategy for developing POM-based MOFs with enhanced proton conductivity. *Inorg. Chem.* **2025**, *64*, 19933–19938.

[11] Ma, J.; Li, X. H.; Xu, N.; Zhang, Z.; Sun, C.; Wang, X. L. pH-induced octamolybdate-based metal-organic complexes with different coordinated metal centers for catalytic epoxidation reaction of alkenes. *J. Catal.* **2025**, *452*, 116444.

[12] Li, F. C.; Li, X. L.; Pan, Y. Z.; Gao, C. L.; Yang, Q. X. Two reduced phosphomolybdate-based metal-organic complexes modified by tunable bis-1*H*-benzimidazole ligands for enhanced photocatalytic Cr(vi) reduction. *Dalton Trans.* **2025**, *54*, 15073–15083.

[13] Chen, H. H.; Ma, X. Y.; Xu, H. J.; Ma, P. T.; Wang, J. P.; Niu, J. Y. Polytantalotungstates stabilized iron catalysts for carbonylation of benzylic C–H bonds. *Inorg. Chem.* **2025**, *64*, 18714–18722.

[14] Li, J. X.; Yang, M. L.; Tian, A. X.; Cao, X. X.; Ying, J.; Wang, X. L. Direct electron transfer from electron-reservoir sandwich-type polyoxometalate to Co2Ni2-cluster via water-assisted proton channels and tandem effects for efficient nitrate-to-ammonia electrocatalysis. *Chem. Eng. J.* **2025**, *521*, 166862.

[15] Wang, C.; Cheng, Y. K.; Bao, L. Y.; Cui, Y. Z.; Liu, Q. Q.; Ma, J. X.; Su, Z. M.; Wang, Z. Q.; Zang, H. Y. Artificial optoelectronic synapse based on purely inorganic polyoxometalates crystalline materials enabling reservoir computing and neuromorphic vision. *Small* **2025**, *21*, 2502601.

[16] Liu, Q. Q.; Li, J. J.; Liu, S. L.; Yu, S.; Chen, Z.; Ma, J. X.; Chen, Y. Z.; Zang, H. Y. Carboxylate-directed self-assembly of $[Mo_2O_4]^{2+}$ units for enhanced proton conduction. *Inorg. Chem.* **2025**, *64*, 16623–16631.

[17] Yang, Y. X.; Zhao, W. L.; Liu, Y. B.; Wang, Q.; Song, Z. H.; Zhuang, Q. H.; Chen, W.; Song, Y. F. Polyoxometalate clusters confined in reduced graphene oxide membranes for effective ion sieving and desalination. *Adv. Sci.* **2024**, *11*, 2402018.

[18] Zhu, M. H.; Iwano, T.; Tan, M. J.; Akutsu, D.; Uchida, S.; Chen, G. Y.; Fang, X. K. Macrocyclic polyoxometalates: Selective polyanion binding and ultrahigh proton conduction. *Angew. Chem., Int. Ed.* **2022**, *61*, e202200666.

[19] Liu, J.; Jiang, N.; Lin, J. M.; Mei, Z. B.; Dong, L. Z.; Kuang, Y.; Liu, J. J.; Yao, S. J.; Li, S. L.; Lan, Y. Q. Structural evolution of giant polyoxometalate: From "Keplerate" to "Lantern" type Mo_{132} for improved oxidation catalysis. *Angew. Chem., Int. Ed.* **2023**, *62*, e202304728.

[20] Ying, J. D.; Liu, T. C.; Wang, Y. Q.; Guo, M.; Shen, Q.; Lin, Y. Q.; Yu, J. G.; Yu, Z. X. Perspectives on membrane development for high temperature proton exchange membrane fuel cells. *Energy Fuels* **2024**, *38*, 6613–6643.

[21] Qi, W.; Wu, L. X. Polyoxometalate/polymer hybrid materials: Fabrication and properties. *Polym. Int.* **2009**, *58*, 1217–1225.

[22] Harilal; Nayak, R.; Ghosh, P. C.; Jana, T. Cross-linked polybenzimidazole membrane for PEM fuel cells. *ACS Appl. Polym. Mater.* **2020**, *2*, 3161–3170.

[23] Mishra, S.; Mishra, S.; Sharma, V.; Kulshrestha, V. High performance interpenetrating network type proton exchange membranes for PEM water electrolysis. *Adv. Sustain. Syst.* **2025**, *9*, e00166.

[24] Namdar, H.; Crespi, E.; Bisello, A.; Speranza, G.; Gottardi, G.; Laidani, N.; Gamba, G.; Testi, M. Performance of catalyst coated sulfonated poly ether ether ketone membrane in PEM water electrolysis: Effects of membrane modification by inclusion of MoS_2-coated carbon nanotubes. *Int. J. Hydrogen Energy* **2025**, *130*, 324–336.

[25] Xu, F.; Chen, Y. B.; Li, J.; Han, Y. Y.; Lin, B. C.; Ding, J. N. Robust poly(alkyl-fluorene isatin) proton exchange membranes grafted with pendant sulfonate groups for proton exchange membrane fuel cells. *J. Membr. Sci.* **2022**, *664*, 121045.

[26] Zeng, M. H.; Liu, W. Q.; Guo, H. K.; Li, T. T.; Li, Q. J.; Zhao, C. J.; Li, X. J.; Li, H. L. Polyoxometalate-cross-linked proton exchange membranes with post-assembled nanostructures for high-temperature proton conduction. *ACS Appl. Energy Mater.* **2022**, *5*, 9058–9069.

[27] Lin, S. Y.; Wang, Y. X.; Dong, X. K.; Cui, Y. W.; Dou, H. X.; Niu, Z.; Wang, L.; Gao, J. S.; He, Y. Sulfonated graphene oxide for proton exchange membranes with significantly enhanced proton conductivity. *Carbon Lett.* **2025**, *35*, 1731–1740.

[28] Fang, F. F.; Zhao, S. X.; Zhang, W.; Zhang, C. Y.; Min, L. F.; Wang, Y. X. Electrophoretic fabrication of proton exchange membranes in fuel cells. *J. Membr. Sci.* **2018**, *565*, 179–185.

[29] Liu, M.; Zhou, S. Q.; Hu, J. B.; Chen, Y. N.; Tong, L. F.; Liu, S. N.; Liu, X. B. Synergistic enhancement of proton conductivity in proton exchange membranes via acid-base cross-linked dual proton channels. *ACS Appl. Polym. Mater.* **2025**, *7*, 17087–17099.

[30] Ma, Y. N.; Tang, S. H.; Zou, Z. G.; Zhang, Y. Q.; Zhu, H. F.; Zhang, Y. L.; Zhang, P. L.; Tang, K. W.; Qiang, Y. Q. A novel polyetherimide hydrogel proton exchange membrane. *New J. Chem.* **2024**, *48*, 9414–9418.

[31] Bai, X. T.; Cao, L. H.; Ji, C.; Zhao, F.; Chen, X. Y.; Cao, X. J.; Huang, M. F. Ultra-high proton conductivity iHOF based on guanidinium arylphosphonate for proton exchange membrane fuel cells. *Chem. Mater.* **2023**, *35*, 3172–3180.

[32] ElHakim, A. A. A.; Awad, S.; Radwan, M. F.; Abdel-Hady, E. E.; ElKousy, S. M. Preparation and characterization of proton exchange membrane by UV photografting technique. *J. Solid State Electrochem.* **2019**, *23*, 2813–2824.

[33] Liu, F. X.; Wang, S.; Li, J. S.; Tian, X.; Wang, X.; Chen, H.; Wang, Z. Polybenzimidazole/ionic-liquid-functional silica composite membranes with improved proton conductivity for high temperature proton exchange membrane fuel cells. *J. Membr. Sci.* **2017**, *541*, 492–499.



Wen-Hang Guo is a Ph.D. candidate at the College of Chemistry, Northeast Normal University, whose research focuses on the design and synthesis of polyoxometalate-based materials and systematic supramolecular assembly.



Feng-Zhi Wang is a Master's graduate from the College of Biological and Agricultural Engineering, Jilin University, whose research focuses on the design and preparation of composite membranes with high proton conductivity.



Chen Wang is a Lecturer at the College of Chemistry and Chemical Engineering, Huangshan University. His research primarily focuses on the design and synthesis of polyoxometalate-based materials and electrochemical energy storage. He has published over 10 academic papers in journals such as *Advanced Materials*, *Small*, *Electrons*, and *Dalton Transactions*.



Song Liang is the Professor and Doctoral Supervisor at Jilin University, specializing in biomimetic microreactors, catalysis, and functional biomimetic medical materials. His research covers the design and assembly of biomimetic microreactors, photo- and electrocatalysis, composite enzymatic catalysis, artificial skin and synthetic patches, and 3D printing of biomimetic hydrogels. He has led projects from NSFC and the Ministry of Education, published over 20 SCI papers, been granted 3 invention patents, and co-authored an English monograph.



Hong-Ying Zang is the Professor and Doctoral Supervisor at Northeast Normal University, and a recipient of the Excellent Young Scientists Fund of the National Natural Science Foundation of China. Her research focuses on the synthesis and assembly of polyoxometalate clusters and their fundamental applications in energy conversion and storage, specifically including the ion-conduction properties of POM-based solid-state materials, the roles of POM materials in energy conversion reactions (HER, ORR, and NRR), and the fabrication of energy-storage devices using POMs as redox mediators. She has led projects funded by the National Natural Science Foundation of China (including the Excellent Young Scientists Fund and the General Program) and the Science and Technology Department of Jilin Province. She has published over 100 SCI-indexed papers, with her research findings appearing in high-impact international journals such as *Nature Chemistry*, *Journal of the American Chemical Society*, *Angewandte Chemie International Edition*, and *Advanced Materials*.

Open Access This article is licensed under the terms of the Creative Commons Attribution 4.0 International License (http://creativecommons.org/licenses/by/4.0/), which permits use, sharing, distribution and reproduction in any medium, provided the original work is properly cited.

© The author(s) 2026. Published by Tsinghua University Press.